

Optimizing for generalization in the decoding of internally generated activity in the hippocampus

Authors: Matthijs A. A. van der Meer^{1*}, Alyssa A. Carey¹, Youki Tanaka¹

¹Department of Psychological and Brain Sciences, Dartmouth College, USA

*Correspondence should be addressed to MvdM. Current address: Department of Psychological and Brain Sciences, Dartmouth College, Hanover, NH 03755. E-mail: [mvdm -at- dartmouth -dot- edu](mailto:mvdm-at-dartmouth-dot-edu).

Running head: Decoding hippocampal sequences

Keywords: encoding, replay, hippocampal sequences, cross-validation, Bayesian

Number of pages: 31

Number of Figures: 9

Number of Tables: 1

1 **Abstract**

2 The decoding of a sensory or motor variable from neural activity benefits from a known ground truth against
3 which decoding performance can be compared. In contrast, the decoding of covert, cognitive neural activity,
4 such as occurs in memory recall or planning, typically cannot be compared to a known ground truth. As a
5 result, it is unclear how decoders of such internally generated activity should be configured in practice. We
6 suggest that if the true code for covert activity is unknown, decoders should be optimized for generalization
7 performance using cross-validation. Using ensemble recording data from hippocampal place cells, we show
8 that this cross-validation approach results in different decoding error, different optimal decoding parameters,
9 and different distributions of error across the decoded variable space. In addition, we show that a minor
10 modification to the commonly used Bayesian decoding procedure, which enables the use of spike density
11 functions, results in substantially lower decoding errors. These results have implications for the interpreta-
12 tion of covert neural activity, and suggest easy-to-implement changes to commonly used procedures across
13 domains, with applications to hippocampal place cells in particular.

14 Introduction

15 The decoding of neural activity is a powerful and ubiquitous approach to understanding information process-
16 ing in the brain. Decoding is typically cast as a mapping from neural data to a sensory or motor variable,
17 such as the identity of a visually presented object or the reaching direction of a motor action; the same idea
18 can be applied to more abstract or even hidden states such as context or past history. By comparing a de-
19 coded (“reconstructed”) variable with the actual value, the contributions of features such as spike timing,
20 adaptation, and correlations to decoding accuracy can be quantified (Nirenberg and Latham, 2003; Panzeri
21 et al., 2015; Schneidman, 2016). Based on the nature and accuracy of the decoder output under various con-
22 ditions, inferences may be drawn about the possible functions of neural populations carrying such signals
23 and the circuitry responsible for generating them (Georgopoulos et al., 1986; Bialek et al., 1991; Pillow et al.,
24 2008). These decoding approaches share the property that when a known stimulus value is available along
25 with neural data, decoding performance can be optimized relative to a known “ground truth” (i.e. the actual
26 stimulus value).

27 Increasingly so, however, decoding is also applied to brain activity occurring in the *absence of any overt*
28 *stimulus or action* (Georgopoulos et al., 1989; Johnson et al., 2009; King and Dehaene, 2014). Such inter-
29 nally generated activity occurs, for instance, during processes such as planning, deliberation, visual imagery
30 and perspective-taking, memory recall and sleep. A well-studied example is provided by studies of hip-
31 pocampal activity recorded in rodents, which exhibits internally generated sequences of neural activity that
32 appear to depict behavioral trajectories during sleep and wakeful rest (“replay”; Skaggs and McNaughton
33 1996; Nadasdy et al. 1999; Davidson et al. 2009; Pfeiffer and Foster 2013), and during the theta rhythm while
34 task-engaged (“theta sequences”, Foster and Wilson 2007; Gupta et al. 2012; Chadwick et al. 2015). Replay
35 is thought to reflect an off-line consolidation process from a fast-learning, episodic-like short-term memory
36 trace in the hippocampus into a semantic-like neocortical knowledge structure (McClelland et al., 1995; Káli
37 and Dayan, 2004; Girardeau et al., 2009; Carr et al., 2011), but also plays a role in on-line task performance,
38 and can depict trajectories that are not well explained by consolidation processes, such as those towards a

39 behaviorally relevant goal and never-experienced paths (O’Neill et al., 2006; Jadhav et al., 2012; Dragoi and
40 Tonegawa, 2013; Ólafsdóttir et al., 2015). Theta sequences may enable one-shot learning, and/or play a role
41 in on-line prediction during behavior (Lisman and Redish, 2009; Malhotra et al., 2012; Feng et al., 2015).

42 How should we interpret the *content* of such internally generated activity? The intuition that replay has a
43 clear resemblance to activity observed during active behavior can be formalized by simply applying the same
44 decoder used to decode activity during overt behavior (Tatsuno et al., 2006; Kloosterman, 2012; Shirer et al.,
45 2012). However, in the rodent hippocampus there are also obvious differences between the two types of
46 activity, such as the compressed timescale and different instantaneous population firing rates (Skaggs and
47 McNaughton, 1996; Lee and Wilson, 2002; Buzsáki, 2015). More generally, there is now overwhelming
48 evidence that hippocampal “place cells” are better viewed as encoding many possible stimulus dimensions
49 rather than just place; these may include relatively low-level properties such as running speed, information
50 about objects and events, and complex history- and context-dependence (Huxter et al., 2003; Lin et al., 2005;
51 McKenzie et al., 2014; Allen et al., 2016). Thus, it is unlikely that the mapping between neural activity and
52 encoded location (the “encoding model”) remains the same between overt and covert epochs, raising the
53 possibility of biases in our ability to decode specific stimulus values, such as different positions along a
54 track.

55 To address the above issues, we provide several practical improvements to commonly used decoding pro-
56 cedures, of particular use for applications to internally generated activity. In acknowledgment of the likely
57 different encoding model in force during overt and covert neural activity, we emphasize that decoding per-
58 formance should be optimized for generalization performance (i.e. to do well on withheld data not used to
59 estimate the parameters of the decoder). We compare different splits of the data, and show that these not
60 only result in different overall decoding accuracy, but also in different accuracy distributions over the stim-
61 ulus space. In particular, these nonuniformities (biases) in accuracy only become apparent when optimizing
62 for generalization to data not included in the training set. Because decoding internally generated activity also
63 involves such generalization, the interpretation of decoding such activity should be informed by the known

64 shape of this bias. Finally, we show that regardless of the type of split used, decoding accuracy can be im-
65 proved by relaxing the assumption of integer spike counts used in the common Bayesian decoding procedure
66 (Zhang et al., 1998; Johnson and Redish, 2007; Pfeiffer and Foster, 2013).

67 **Materials and Methods**

68 **Overview**

69 Our aim is to describe how the output of decoding hippocampal ensemble activity depends on the configu-
70 ration of the decoder. In particular, we examine two components: (1) the split between training and testing
71 data, and (2) the parameters associated with the estimation of firing rates and tuning curves (the encoding
72 model). Both are described in the *Analysis* section. All analyses are performed on multiple single unit data
73 recorded from rats performing a T-maze task, described in the *Behavior* section. Data acquisition, annotation,
74 and pre-processing steps are described in the *Neural data* section.

75 All preprocessing and analysis code is publicly available on our GitHub repository, <https://github.com/vandermeerlab/papers>. Data files are available from our lab server on request by e-mail to the
76 corresponding author.

78 **Neural data**

79 **Subjects and overall timeline.** Four male Long-Evans rats (Charles River and Harlan Laboratories), weigh-
80 ing 439-501 g at the start of the experiment, were first introduced to the behavioral apparatus (described
81 below; 3-11 days) before being implanted with an electrode array targeting the CA1 area of the dorsal hip-

82 pocusampus (details below). Following recovery (4-9 days) rats were reintroduced to the maze until they ran
83 proficiently (0-3 days), at which point daily recording sessions began. On alternate days, rats were water-
84 or food-restricted. In parallel with the maze task, some rats (R042, R044, R050) were trained on a simple
85 Pavlovian conditioning task in a separate room (data not analyzed).

86 **Behavioral task.** The apparatus was an elevated T-maze, constructed from wood, painted matte black with
87 white stripes applied to the left arm (Figure 1) and placed on a metal frame approximately 35 cm in height.
88 The distance from the start of the central stem to the ends of the arms was 272 cm (R042) or 334 cm (R044,
89 R050, R064; these numbers are subject IDs). 6% sucrose (~0.1 ml) was dispensed upon reaching the end of
90 the left arm, and food (5 pellets of Test Diet 5TUL 45 mg pellets) was dispensed upon reaching the end of
91 the right arm.

92 Daily recording sessions consisted of (1) a pre-behavior recording epoch, taken as the animal rested on a
93 recording pedestal (terracotta pot lined with towels; 20-30 min), (2) approximately 20 trials on the maze, with
94 an intertrial interval (30-240 s) on the recording pedestal after each trial, and (3) a post-behavior recording
95 epoch (10-20 min). A trial was defined as a run from the starting point at the base of the central stem to
96 one of the reward locations; photobeams at the track ends were used to find pairs of crossings defining the
97 shortest interval between leaving the base and arriving at an end. Only data from runs on the track were
98 analyzed here.

99 Because rats were food- or water-restricted, they tended to prefer choosing the arm leading to the reward to
100 which their access was limited. On some sessions, access to a preferred arm was blocked with a movable
101 barrier to ensure sampling of the non-preferred arm (forced choice). Trials on which the animal turned
102 around, or exhibited other disruptive behaviors (climbing on the barrier, extended grooming, etc.) were
103 excluded from analysis.

104 **Electrode arrays and surgery.** Subjects were each implanted with a single-bundle microelectrode array

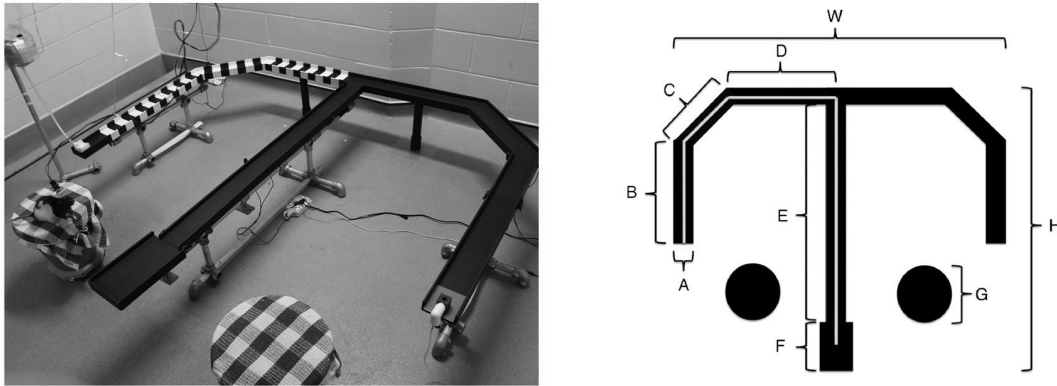


Figure 1: Behavioral apparatus. In daily recording sessions, rats ran approximately 20 trials on an elevated T-maze. Trials were free-choice except for a small number of forced trials in which access to one of the arms was prevented by a barrier to ensure that at least 5 trials for both left and right arms were available for each session. Track dimensions were: width 10 cm (A), total maze height 167 cm (H), total maze width 185 cm (W), total path length 334 cm (white trajectory, R042 excepted, who had a shorter B segment for a total path length of 285 cm).

105 targeting the CA1 region of dorsal hippocampus in the right hemisphere (AP -4.0mm, ML +2.5mm). R042
106 and R044 were each implanted with a 15-tetrode 1-reference array, and R050 and R064 were each implanted
107 with a 16-tetrode 4-reference array. Surgical procedures were as described previously (Malhotra et al., 2015).
108 Briefly, the skull was exposed and a ground screw was placed through the contralateral parietal bone. Arrays
109 were lowered to the surface of the cortex through a craniotomy, and the remaining exposed opening was
110 sealed with a silicone polymer (KwikSil). Then, the arrays were anchored to the skull using small screws
111 and acrylic cement. Rats were given a minimum recovery period of four days, during which antibiotics and
112 analgesics were administered, before retraining began. Tetrodes were slowly advanced to the CA1 layer
113 over a period of 4-9 days. The first recording sessions began no sooner than nine days after surgery. All
114 procedures were performed in accordance with the Canadian Council for Animal Care (CCAC) guidelines,
115 and pre-approved by the University of Waterloo Animal Care Committee (protocol 10-06).

116 **Recording methods.** Neural activity from all tetrodes and references was recorded on a Neuralynx Digital
117 Lynx SX data acquisition system using HS-36-LED analog buffering headstages tethered to a motorized
118 commutator. Local field potentials, filtered between 1-425 Hz, were continuously sampled at 2 kHz. Spike
119 waveforms, filtered between 600-6000 Hz, were sampled at 32 kHz for 1 ms when the voltage exceeded an
120 experimenter-set threshold (typically 40-50 μ V) and stored for offline sorting. Acquired signals for all rats
121 (except R042, whose data was recorded relative to animal ground) were referenced to an electrode located
122 in the corpus callosum, dorsal to the target recording site. A video tracking algorithm recorded the rat's
123 position based on headstage LEDs picked up by an overhead camera, sampling at 30 Hz. All position data
124 was linearized by mapping each 2-dimensional position sample onto the nearest point of an ideal linearized
125 trajectory on the track, drawn for each session by the experimenter. Position samples further than 25cm from
126 this idealized trajectory were treated as missing values.

127 **Preprocessing and annotation.** Signals were preprocessed to exclude intervals with chewing artifacts and
128 high-amplitude noise transients where necessary. All spiking data was initially clustered into putative units
129 automatically (KlustaKwik, K. D. Harris) and then manually checked and sorted (MClust 3.5, A. D. Re-
130 dish). Highly unstable units and units that fired fewer than 100 spikes in a recording session were excluded.
131 Recording locations were histologically confirmed to lie in the dorsal CA1 cell layer. A total of 2017 units
132 were recorded from 4 rats across 24 sessions (Table 1); 889 of these were units were rated as questionable
133 isolation quality by the experimenter and kept separate for later analysis.

134 **Inclusion criteria.** Recording sessions with at least 20 units firing a minimum of 25 spikes during "run"
135 epochs (used for tuning curve estimation, described below) for both left and right trials separately were
136 included for analysis. This left out five sessions (four from R044, one from R042) resulting in a total of 19
137 sessions eligible for analysis.

Rat ID	Session 1	Session 2	Session 3	Session 4	Session 5	Session 6	Total
R042	22 (13)	74 (39)	107 (40)	64 (43)	73 (40)	59 (31)	399 (206)
R044	17 (11)	13 (9)	43 (21)	53 (26)	50 (27)	41 (22)	217 (116)
R050	72 (42)	94 (40)	72 (28)	113 (44)	128 (36)	112 (46)	591 (236)
R064	121 (59)	136 (47)	116 (52)	162 (45)	178 (68)	151 (60)	864 (331)

Table 1: Total neural units for each rat across each of their six recording sessions. Numbers in parentheses indicate how many of the numbers listed were units rated as questionable. Sessions listed in italics were excluded due to insufficient number of recorded units.

138 Analysis

139 **Overview.** Our main approach is to employ a standard memoryless Bayesian decoder, common to all anal-
140 yses and described below. We will vary first, the nature of different splits in the data between “training” and
141 “testing”, and second, parameters associated with the estimation of input firing rates (spike density functions)
142 and input tuning curves (the “encoding model”). In all these cases, the output of the decoding procedure is,
143 for each time bin, a probability distribution over (linearized) position, given the observed spiking activity.

144 **Bayesian decoding.** We use the canonical Bayesian decoder (Brown et al., 1998; Zhang et al., 1998),
145 specifically the one-step, “memoryless” version with a uniform spatial prior. This procedure (reviewed in
146 detail elsewhere; Johnson et al. 2009; van der Meer et al. 2010; Kloosterman et al. 2014), along with the key
147 parameters varied in this study, is illustrated in Figure 2. The decoded location \hat{x} for a given time bin we took
148 to be the mode of the posterior (location with the highest probability; maximum a posteriori). A decoding
149 error can then be defined as the distance to the true position $E_{bins}(t) = |x(t) - \hat{x}(t)|$. Because x has the unit
150 of bins, this quantity is converted into a worst-case error in centimeters as follows: $E_{cm}(t) = E_{bins} * b + \frac{b}{2}$,
151 where b is the bin size in cm (we used 3 cm for the results reported here, and a time bin $\tau = 25$ ms). Both
152 the estimation of tuning curves (the encoding model, described below) and the decoding of spike data were

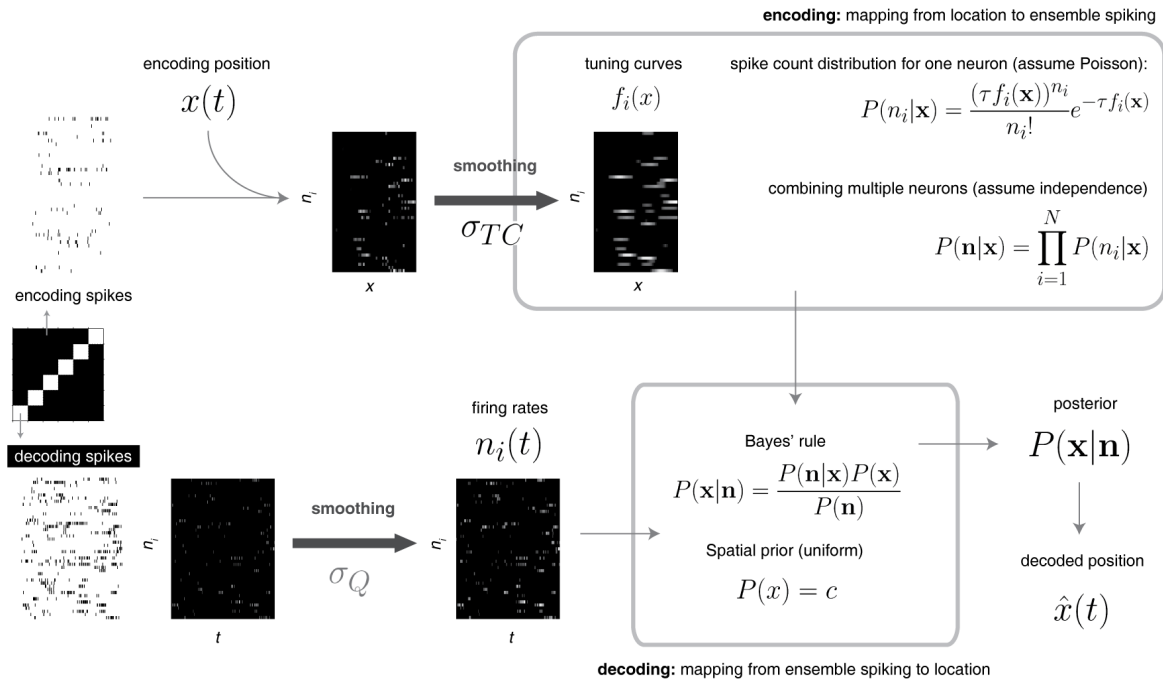


Figure 2: Schematic of the Bayesian decoding scheme. The overall workflow follows the canonical procedure based on the common assumptions of Poisson-distributed spike counts around mean firing rates given by stable tuning curves, and independence between neurons. Crucial variables in the results reported here are (1) the split in the data between trials used for estimating tuning curves (“encoding spikes”) and trials used for decoding (“decoding spikes”; see Figure 3 for a detailed explanation), (2) the width of the Gaussian kernel σ_{TC} used to smooth the tuning curves (the empirically determined mapping from location to firing rate for each recorded neuron), and (3) the width of the Gaussian kernel σ_Q used to obtain the spike density functions used as the input to the decoder.

153 restricted to data when the animal was running (≥ 5 cm/s).

154 We use this decoding procedure here because it has become the *de facto* standard in the hippocampal place
 155 cell literature (Kloosterman et al., 2014; Silva et al., 2015; Grosmark and Buzsaki, 2016); however, the
 156 manipulations in the present study (discussed below) are general and can be straightforwardly applied to
 157 other decoding methods such as optimal linear decoding, regression-based methods and general-purpose

158 classifiers such as support vector machines, et cetera (Pereira et al., 2009; Pillow et al., 2011; Deng et al.,
159 2015).

160 **Cross-validation.** The data used for the estimation of the encoding model (tuning curves; “training data”)
161 may be the same as the data used for decoding and error estimation (“testing data”), but this need not be
162 the case (Figure 3). We systematically compare different splits between training and testing data, focusing
163 on three specific cases: same-trial decoding (decode each individual trial based on tuning curves obtained
164 from that same trial; Figure 3A), next-trial decoding (decode each individual trial based on tuning curves
165 from the *next* trial; Figure 3C) and leave-one-out decoding (decode each trial based on tuning curves from
166 all trials except the one being decoded; Figure 3D). Decoding errors reported are always for a specific split
167 and this will be reported in the text; note that for all splits used here, each trial is decoded separately, using
168 tuning curves obtained from a set of encoding trials specific to the trial being decoded (this is unlike all-to-all
169 decoding, Figure 3B, in which the same set of all encoding trials is used for every decoding trial). Left and
170 right trials were always treated separately, i.e. only left trials are used to decode left trials, and the same for
171 right trials.

172 **Firing rate estimation.** Strictly speaking, Bayesian decoding based on the assumption that firing rates are
173 Poisson-distributed requires integer spike counts for the estimation of $P(s|x)$ (Figure 2). However, this
174 means that there will be effects of binning, which will become more prominent as the time window (bin) size
175 τ becomes smaller. For instance, if bins only contain 0 or 1 spike, then which side of a bin edge a spike falls
176 on can potentially have a large effect. This issue is prominent in many aspects of spike train analysis, and is
177 typically addressed by convolving the raw spike train to obtain a *spike density function* (*SDF*), an estimate
178 of firing rate which varies continuously in time (Cunningham et al., 2009; Kass et al., 2014).

179 To make the standard Bayesian decoding equations compatible with non-integer spike density functions,
180 we note that the denominator $n_i!$ does not depend on x and can therefore be absorbed into a normalization
181 constant C which guarantees that $\sum_x P(n_i|x) = 1$ (Eq. 36 in Zhang et al. 1998). For the results presented

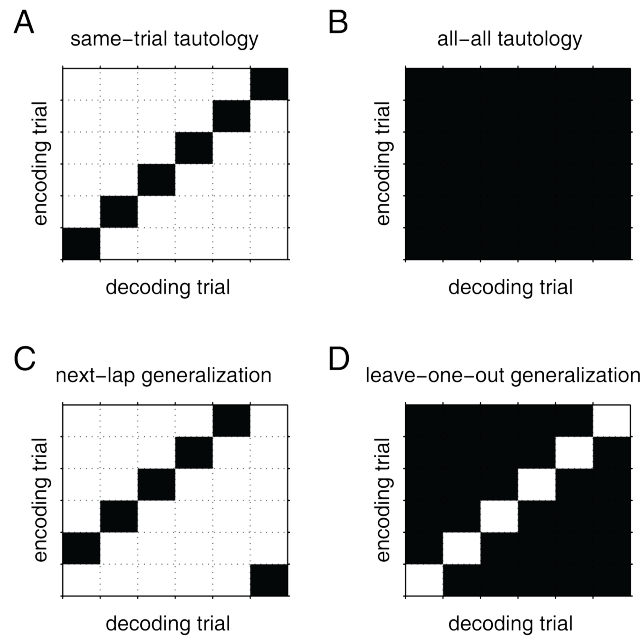


Figure 3: Schematic of different splits between data used for estimating the encoding model (tuning curves, “training data”) and data used for evaluating decoding accuracy (“testing data”). Data splits in the **top row** are “tautological” in that tuning curves are estimated on the same data used for decoding. In contrast, data splits on the **bottom row** measure generalization performance (cross-validation) in the sense that the decoding data was not included in the data used for estimating the encoding model. **Black** cells in the matrices shown indicate trials used to estimate the encoding model. Thus, for instance, the left column in **C** shows that to decode trial 1, tuning curves were estimated from trial 2.

182 here, we obtain spike density functions by convolving raw spike trains with a Gaussian kernel with SD σ_Q ,
183 discretized at a resolution of 25 ms (the τ in Figure 2).

184 A possible side effect of using this procedure on the decoding spikes only (i.e. not on the spikes used to
185 estimate the tuning curves, described below) is that firing rate-stimulus combinations that are inconsistent
186 across the ensemble become more likely, e.g. for every individual location x_i in space, there is at least one
187 neuron that assigns $P(x_i|n) = 0$ (such cases result in the white areas in Figure 4; only sessions in which at
188 least 80% of samples could be decoded were included, except when indicated explicitly in the text). This can

189 be avoided by simply convolving all spikes with the same kernel σ_Q ; here we did not do so in order to show
190 the effects of convolving the decoding spikes independently of the encoding model estimation. Smoothing
191 the tuning curves, as described in the next section, is another effective method of avoiding this issue.

192 **Encoding model estimation.** Bayesian decoding requires an estimate of $P(s|x)$, the probability of observ-
193 ing a firing rate vector s for a given stimulus value x . As in previous work, we assume firing rates are
194 independent between neurons and Poisson-distributed around some mean rate λ ; this simplification means
195 that we only need to know the mean firing rate as a function of the stimulus variable, $\lambda(x)$, for each neuron.
196 These are the *tuning curves*, which taken together across all neurons can be thought of as an *encoding model*,
197 i.e. the mapping from stimulus values to neural activity. We estimate tuning curves non-parametrically from
198 the data by (1) restricting the data to intervals when the animal was running on the track (≥ 5 cm/s; *encod-*
199 *ing spikes* in Figure 2), (2) linearizing the position data and binning in bins of 3 cm, (3) obtaining a firing
200 rate histogram by dividing spike count by occupancy for all bins, and (4) optionally smoothing the resulting
201 tuning curve with a Gaussian kernel of standard deviation σ_{TC} (with units in cm).

202 **Inventory of behavioral and neural measures used.** Figure 9 shows the distribution, across locations, of a
203 number of behavioral and neural measures which we relate to decoding accuracy. We explain how these are
204 computed in turn.

- 205 • *Occupancy* (in seconds; time spent at each location on the track) is computed simply by binning video
206 tracking samples and multiplying the sample counts by the length of each video frame (1/30 s).
- 207 • *Place fields* are detected based on session tuning curves, when a contiguous area of at least 15cm is
208 associated with a minimum firing rate of 5 Hz, and a mean firing rate of no more than 10 Hz. For each
209 field (contiguous area) the location of the field is taken to be the neuron's maximum firing rate in in
210 the field.

- 211 • *Tuning curve variability across trials* (Figure 9E-F) is obtained by taking the standard deviation, across
212 trials within each session, of single-trial tuning curves.

- 213 • *Bootstrapped tuning curve variability* (Figure 9G-H) is computed by generating a distribution of 1000
214 resampled tuning curves, with each sample using a random 90% of the position and spiking data.
215 Specifically, every spike is assigned to the position sample closest in time. Then, after selecting a ran-
216 dom 90% of position samples, those samples and the associated spikes are removed before computing
217 a tuning curve. A measure of tuning curve variability is then obtained by taking the standard deviation
218 across the distribution of resampled tuning curves.

- 219 • *Population vector (PV) correlations* are obtained by correlating, for each location on the track, the
220 tuning curve firing rates (across cells) either between tuning curves obtained from each pair of trials
221 (Figure 9I-J) or between tuning curves from a single trial and the complementary tuning curve of all
222 trials except that one (Figure 9K-L).

223 Results

224 We sought to determine how different configurations of the commonly used one-step Bayesian decoder
225 (Brown et al., 1998; Zhang et al., 1998) relate to the decoding accuracy of position based on ensembles of
226 hippocampal place cells. In particular, we applied different splits to the data, partitioning it into “training”
227 data from which tuning curves were estimated, and “testing” data from which decoding accuracy was de-
228 termined (a type of cross-validation). In addition, we varied parameters associated with the estimation of
229 tuning curves and firing rates (σ_{TC} and σ_Q in Figure 2).

230 Our motivation for exploring different data splits is the question of how internally generated sequences (e.g.

231 “replays”) of neural activity can be decoded in a principled manner. For such sequences, the true mapping
232 from neural activity to stimulus space is generally unknown; after all, there is no true stimulus value to which
233 decoded output can be compared. Under these conditions, decoders should be optimized for generalization
234 performance, i.e. performance on “testing” data not used to “train” the decoder. In statistics and machine
235 learning, such cross-validation is routinely used to prevent overfitting (Hawkins, 2004; Alpaydin, 2014).
236 Applied to the problem of decoding covert sequences, this concept suggests that we choose the decoder
237 which performs best on input data from trials not included in the estimation of tuning curves. Thus, we use
238 data from withheld trials as a proxy for internally generated sequences, such that we can estimate how well
239 various decoders are likely to perform on actual covert sequences.

240 Specifically, applied to decoding neural data collected across a number of repeated trials, as is the case here
241 in rats running a T-maze task (Figure 1), a number of different splits between testing and training data are
242 possible, illustrated in Figure 3. A commonly used approach in the hippocampal place cell literature is to
243 not perform any split at all, i.e. to estimate tuning curves based on the full data set, and use those to decode
244 the full data set (Figure 3B, Johnson and Redish 2007; Karlsson and Frank 2009; Pfeiffer and Foster 2013;
245 Zheng et al. 2016). We refer to this approach as “tautological” because the same data is used for both. It
246 is possible to do this at different levels of granularity, for instance going down to the single trial level by
247 decoding each individual trial based on tuning curves from that trial (Figure 3A), while maintaining the
248 property that the same data is used for tuning curve estimation and decoding.

249 **Overall effects of different decoding configurations on accuracy**

250 We found that the best outright decoding performance (as quantified by the error relative to true location)
251 was obtained using such tautological decoding. “Same-trial” decoding performed best of all data splits tested
252 (Figure 4A; average decoding error 5.42 ± 1.02 cm for the best-performing parameters; standard error across
253 subjects). However, if the goal is to optimize decoding performance on trials not included in the training set,

254 the picture changes. Decoding using the *next trial* resulted in a decoding error ~ 4 -fold worse than the same-
255 trial decoding (19.19 ± 2.85 cm; Figure 4B). Leave-one-out decoding was intermediate between these two
256 (11.25 ± 1.58 cm; Figure 4C), a pattern that held across a wide range of decoding parameters (see also
257 Figure 5 for specific comparisons).

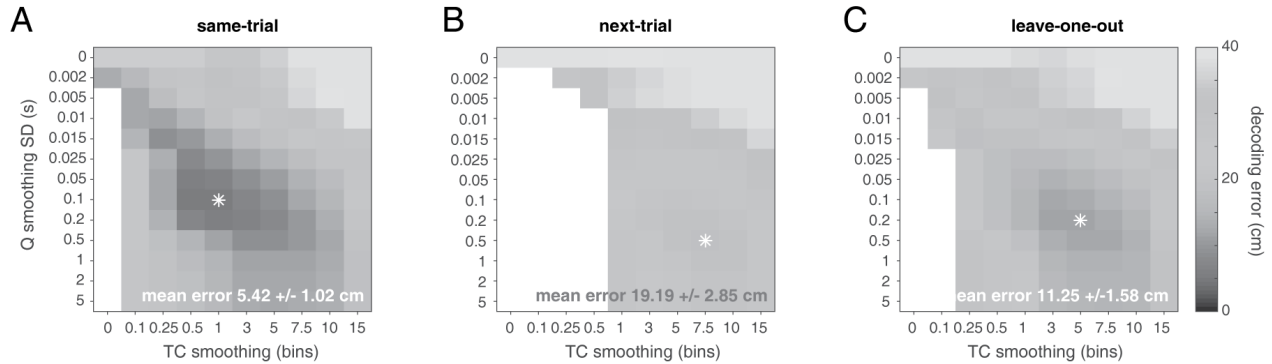


Figure 4: Decoding accuracy for different data splits (**left:** same trial, **middle:** next trial, **right:** leave-one-out) and decoder parameters (vertical axis: standard deviation of Gaussian kernel (in s) used to convolve spike trains, horizontal axis: standard deviation of Gaussian kernel used to convolve tuning curves (in 3 cm bins). Grayscale shows the mean decoding error (in cm) for different parameter and data split combinations. Note that decoding accuracy for some parameter combinations cannot be estimated if temporal smoothing results in decoding spike counts inconsistent with the encoding model (empty data points; see *Methods* for details). Results shown were obtained with a decoding time bin size (τ) of 25 ms; only sessions with at least 20 cells for both left and right trials on the T-maze were included, averaging across left and right trials (19 sessions total). The white asterisk indicates the parameter combination resulting in the lowest mean decoding error; this is the value reported here for each data split, along with the standard error over subjects ($n = 4$).

258 Several other features of Figure 4A-C are worth noting. First, performing no smoothing at all on either the
259 spike trains or the tuning curves (0/0, the data point on the top left of each panel) results in large decoding
260 error. Previous results manipulating the width of the time window indicated minimum error for a time
261 window in the ~ 0.5 -1s range (Zhang et al., 1998) this is confirmed here by the error minimum at 0.2 or 0.5

262 s SD smoothing kernels. Surprisingly however, even very minimal temporal smoothing of the spike trains
263 to be decoded (e.g. a kernel with 5 ms SD) can result in substantial improvements in decoding performance
264 compared to no temporal smoothing (up to 2-fold; see Figure 5 for a close-up of this effect). Second,
265 best decoding accuracy almost invariably required some smoothing of the tuning curves, even when the
266 leave-one-out procedure ensured many trials were used for tuning curve estimation. Third, the parameters
267 yielding optimal decoding accuracy differed between data splits; note for instance how the dark gray area
268 (corresponding to low decoding error) is shifted towards the top left for Figure 4A compared to Figure 4C.
269 Thus, different data splits interact with decoding parameters to produce overall decoding accuracy.

270 To show more clearly the data in Figure 4 for selected parameter combinations of interest, we plotted sep-
271 arately the raw decoding error (Figure 5A-C) and decoding error normalized to same-trial decoding within
272 each recording session (Figure 5D). Including units with questionable isolation quality decreased decoding
273 error across all conditions (compare Figure 5A-B; see Methods and Table 1 for unit counts), and we there-
274 fore used the full set of units including questionable units for all other analyses. Regardless of the set of
275 units used, however, Figure 5 illustrates clearly the large improvement in decoding accuracy of very minimal
276 smoothing (e.g. light dashed line, 5 ms kernel) compared to no smoothing (dark dashed line). Also evident is
277 the performance improvement of the leave-one-out data split over the next-trial data split; this improvement
278 was particularly large for larger smoothing (for which, in turn, overall decoding accuracy was better), for no
279 or minimal smoothing, next-trial and leave-one-out decoding tended not to differ.

280 **Effect of trial numbers on decoding accuracy**

281 Given that leave-one-out decoding performed as well or better than next-trial decoding, we can ask how this
282 effect depends on the number of trials included in the leave-one-out procedure. This can be of practical
283 importance in determining the number of trials of behavioral sampling will be sufficient for decoding dur-
284 ing internally generated activity. Leave-one-out and next-trial decoding can be seen as opposite ends of a

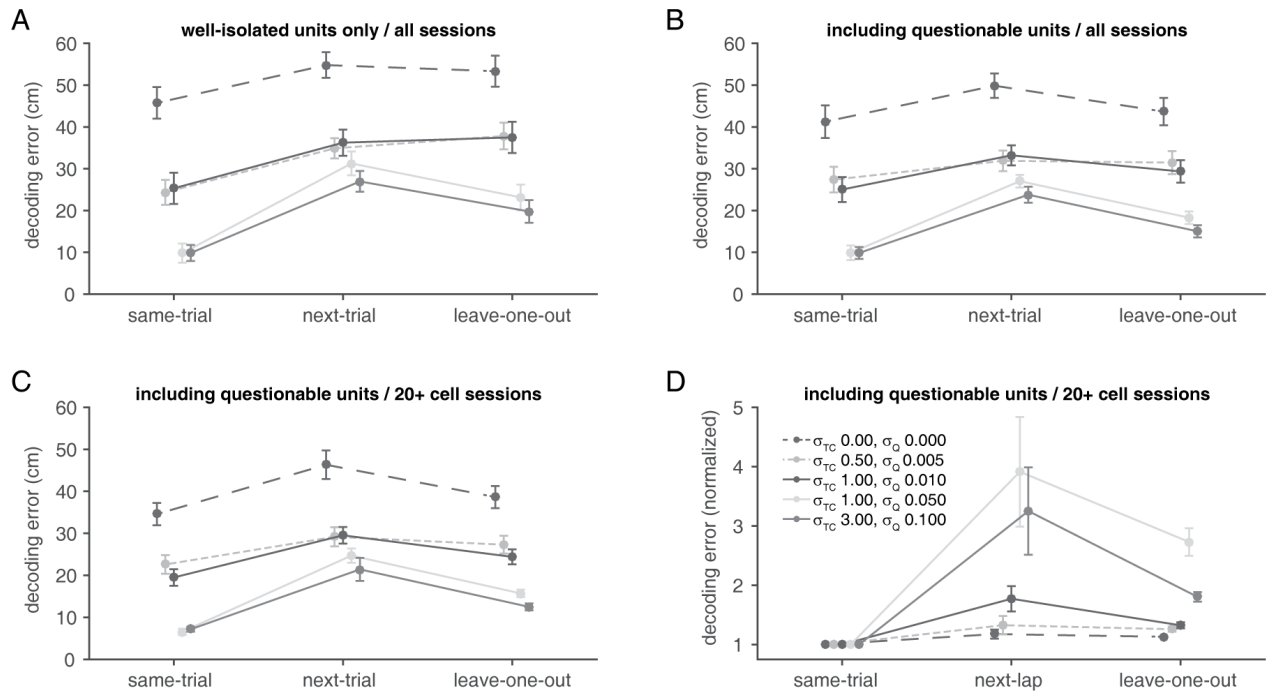


Figure 5: Decoding error for selected parameter and data combinations. Panels **A** and **B** show decoding error run on all sessions ($n = 24$, i.e. without requiring a minimum number of cells to be active) to compare decoding error when only well-isolated units are used (**A**) or when units of questionable isolation quality are included (**B**). Panels **C** and **D** are replots of the same data as in Figure 4, i.e. for sessions with at least 20 cells that met inclusion criteria ($n = 19$; see Methods). For panel **D**, decoding error is normalized on a single-session basis to the same-trial decoding. Errorbars indicate SEM over subjects ($n = 4$).

285 spectrum along which the number of trials used to estimate tuning curves is systematically varied. Overall,
 286 decoding performance increased as more trials were included, with diminishing returns for larger numbers
 287 of trials (Figure 6). As expected from the results in the previous sections, these overall performance gains
 288 in absolute and relative decoding accuracy depended on the amount of smoothing, with the largest gains for
 289 larger smoothing.

290 The results up to this point raise an obvious question: *why* does decoding performance depend on the way the
 291 data is split between encoding and decoding (training and testing) sets? There are two major possibilities.

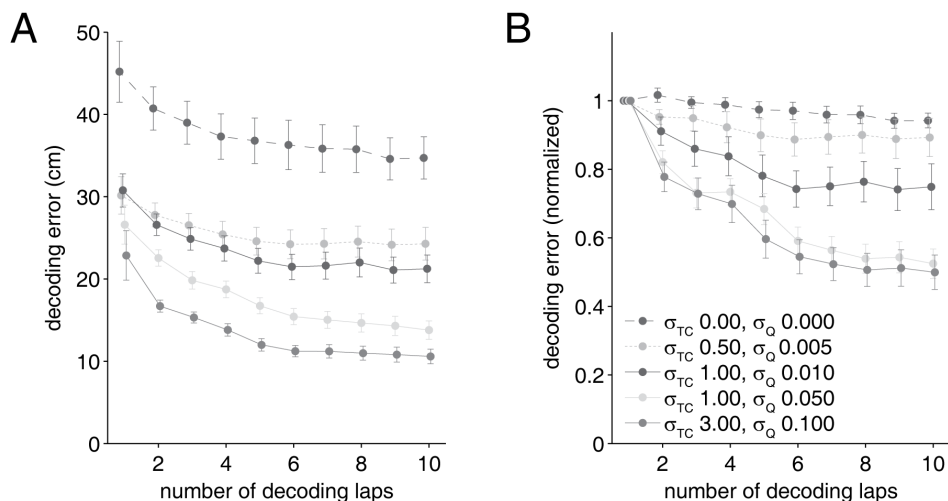


Figure 6: Raw decoding error (**A**) or within-session normalized decoding error (to next-trial decoding error, **B**) as a function of the number of trials included in the cross-validation. Overall, decoding error tended to decrease as more trials were included, but the magnitude of this effect depended on the degree of smoothing used, with stronger smoothing (associated with lower decoding error) benefiting more from including more trials.

292 The first one is overfitting, which assumes that estimating encoding models from a single trial includes
293 fitting a certain amount of noise which generalizes poorly to other trials. In this scenario, including more
294 trials would lead to averaging out of some of this noise, improving performance as shown above (Figure
295 6). However, a further, non-exclusive possibility is that the encoding model (the mapping between position
296 along the track and neural activity) is not constant across trials. To test this idea, we plotted single-trial
297 decoding performance as a function of the “distance” between the encoding and decoding trials (this can
298 be visualized by shifting the matrix in Figure 3C horizontally, away from its shown configuration with a
299 distance of one trial to distances of multiple trials).

300 Figure 7 shows that both raw and relative decoding error (normalized within-session to same-trial decoding)
301 tended to increase with larger distance between the encoding and decoding trial (linear mixed model with
302 subject-specific intercepts; effect of trial distance $F = 10.13$, $p = 0.0017$ for parameters with the smallest
303 effect). In other words, decoding was more accurate when using tuning curves estimated from a “near” trial,

304 compared to using tuning curves from a “far” trial. However, it should be noted that pinpointing the source
305 of this effect is challenging, given that aspects of behavior such as average running speed and path stereotypy
306 tend to change over the course of a session, in a manner likely correlated with trial distance (elapsed time) in
307 this experiment. In attempt to control for such changes, we fitted linear mixed models with subject-specific
308 intercepts to the data with decoding error as the dependent variable for each pair of trials (a decoding “target”
309 trial, and an encoding “source” trial). For each such pair we included not only (1) the trial distance (number
310 of trials) and (2) the time difference (between trial start times) as the key regressors of interest, but also
311 (3) the difference in distance run, and (4) the difference in length (in time) between the trials in the pair.
312 Even after the behavioral variables (3) and (4) were included in the model, either trial distance (1) or time
313 difference (2) dramatically improved model fits (nuisance variables only log likelihood -595.2, pseudo- R^2
314 0.22; trial distance added -566.39, pseudo- R^2 0.40, time difference added -563.71, pseudo- R^2 0.42; all
315 model comparisons $p < 0.001$ for parameters with the smallest effect). This effect suggests that individual
316 trials are associated with distinguishable ensemble firing patterns, potentially reflecting trial-unique aspects
317 of experience (consistent with results from Manns et al. 2007; Mankin et al. 2012; Allen et al. 2012; Ziv
318 et al. 2013). In turn, this observation raises the possibility that a given covert sequence may be best decoded
319 by an encoding model associated with a specific trial.

320 **Decoding accuracy for different locations**

321 The overall decoding error measure examined so far averages across different stimulus (location) values.
322 However, it is possible that different data splits and decoding parameters differentially affect decoding accu-
323 racy for specific locations. Testing whether any such nonuniformity exists in the data is crucial when making
324 comparisons between decoding covert variables (replay) across different stimulus ranges, such as different
325 parts of a track. To test if this occurs, we computed the decoding error as a function of location on the track
326 (Figure 8A-B). Apart from the overall difference in raw decoding error across data splits, there were clear
327 differences in how error was distributed *across* locations: for next-trial and leave-one-out decoding, error

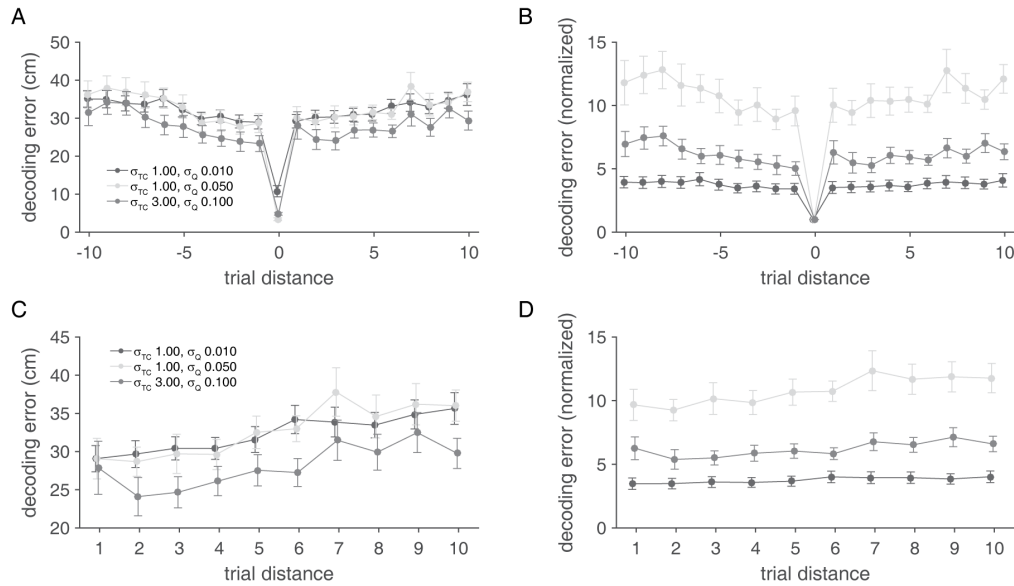


Figure 7: Decoding error as a function of the distance (in number of trials) for single-trials decoding. A trial distance of 0 means that the same trial is used for encoding (estimating tuning curves) and decoding; a trial distance of +1 means that the next trial is used for encoding, and so on. Raw decoding error (**A**) and decoding error normalized within sessions to same-trial decoding error (**B**) tended to increase with larger trial distances. **C** and **D** show the same data but for absolute distance, i.e. previous and next-trial decoding are both distance 1. In order to have sufficient numbers of trial pairs to perform this analysis, trial pairs on which at least 20% of samples could be decoded were included (unlike the 80% threshold used for all other results; see *Methods*).

328 tended to increase at the start and end of the track. In contrast, for same-trial decoding, this effect was not
 329 apparent at the start of the track. Smaller differences between the same-trial and leave-one-out were also ap-
 330 parent, such as an increase in decoding error around the choice point. Next, we plotted the confusion matrix
 331 of actual and decoded locations for the different data splits (Figure 8C). Apart from the overall difference in
 332 decoding accuracy, visible as the width of the diagonal, distortions are visible for the leave-one-out case in
 333 particular. The point indicated by the white arrow shows relatively poor decoding at the choice point of the
 334 T-maze, an effect not apparent for the other data splits.

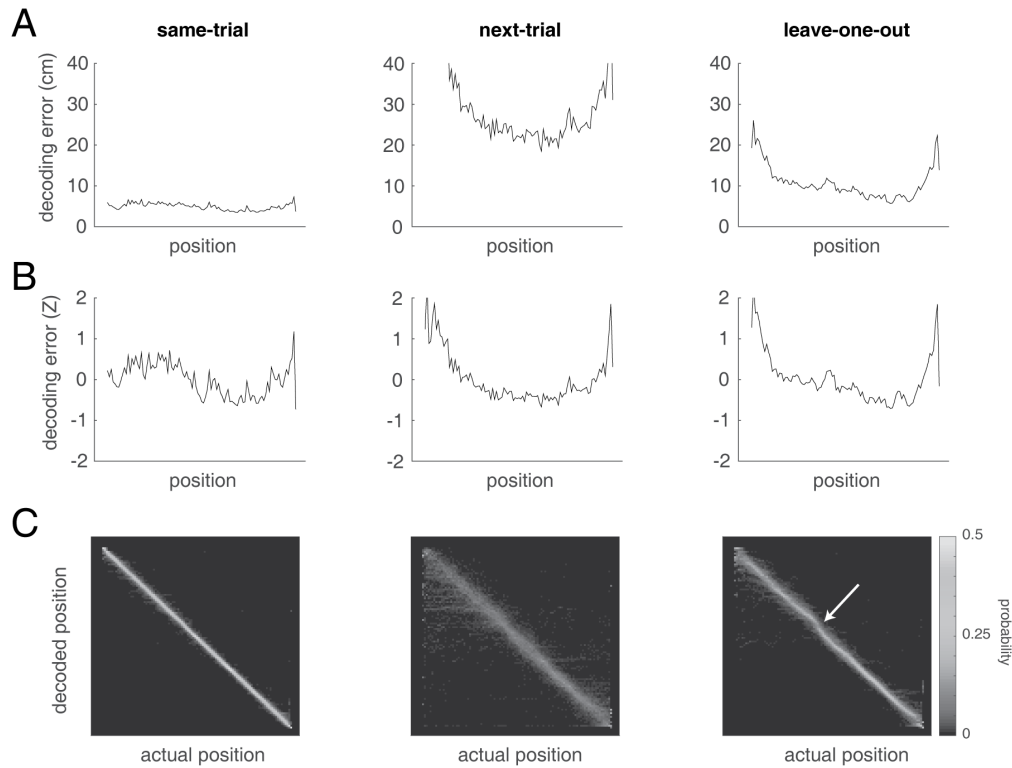


Figure 8: Average decoding error, by location along the track, for the best-performing decoding parameters (starred in Figure 4). Column layout is as in Figure 4), with same-trial decoding on the left, next-trial in the center, and leave-one-out on the right. **A** shows the raw decoding error, **B** shows within-session Z-scored (across space) error. Importantly, these distributions are different; for instance, the next-trial and leave-one-out distributions show increases in error at the start and end of the track not seen in the same-trial distribution. **C:** confusion matrices for actual and decoded position, averaged across sessions. Note the distortion away from the diagonal apparent in the leave-one-out distribution (white arrow) not present in the same-trial case.

335 In general, there are a number of obvious potential explanations for non-uniform distributions of decod-
336 ing accuracy, such as differences in the density of place fields and variability in behavior. However, these
337 would be expected to affect both tautological and cross-validated decoding, when the results show strikingly
338 different patterns of decoding accuracy for those cases (Figure 8B). To determine what aspects of the data
339 could help account for the observed nonuniformity in cross-validated decoding, we plotted several quantities
340 related to behavior and neural activity as a function of location (Figure 9). Both average occupancy and

341 its variability across trials were non-uniform (Figure 9A-B) with more sampling around the midpoint of the
342 track compared to the start and end. The average firing rate of neurons with place fields and the number of
343 place fields across the track also showed distributions that did not seem clearly related to decoding accuracy
344 (Figure 9C-D).

345 Based on the intuition that cross-validated decoding accuracy depends on the degree of consistency in be-
346 havior and neural activity across trials, we computed a number of measures designed to quantify this: (1) the
347 variability in single-trial tuning curves, estimated across trials for each cell individually and then averaged
348 (Figure 9E-F), (2) the variability in entire-session tuning curves, as estimated by a resampling (bootstrap)
349 procedure (Figure 9G-H), and (3) the population vector correlation (i.e. mean firing rates across all cells for
350 a given location), either across single-trial tuning curves or between single-trial tuning curves and the com-
351plementary leave-one-out set of tuning curves (Figure 9I-L). These measures showed different distributions
352 across the track, with variability in estimating session tuning curves (Figure 9G-H) showing a distribution
353 most similar to the observed cross-validated decoding accuracy (Figure 8B). Thus, although multiple factors
354 contribute to decoding accuracy, tuning curve variability (as obtained by a bootstrap) may underlie decoding
355 accuracy differences specific to cross-validated decoding.

356 Discussion

357 This study contributes two advances to the methodology for decoding internally generated neural activity.
358 First, we show that using different data splits for the estimation of the encoding model (tuning curves) and the
359 decoding of hippocampal place cell activity affects decoding performance. Specifically, although same-trial
360 decoding was the clear winner in terms of absolute decoding error, single-trial decoding generalizes poorly,
361 leading to large decoding errors when applied to trials other than the one used to obtain tuning curves. Best
362 generalization performance is obtained with leave-one-out cross-validation. These observations are in line
363 with standard practice in the fields of machine learning and statistics (Bishop, 2006); here we explore the

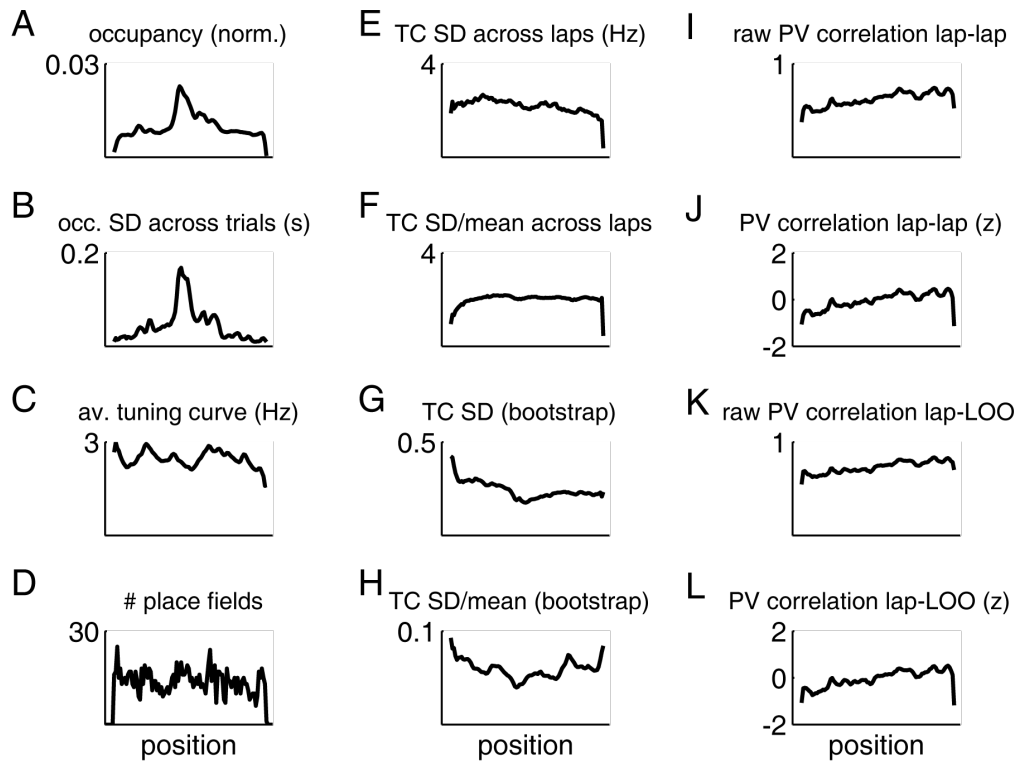


Figure 9: Among several behavioral and neural measures, tuning curve variability as estimated by a bootstrapping procedure is most similar to cross-validated decoding accuracy. **A:** Normalized occupancy (time spent) and its standard deviation across trials within each session (**B**). **C:** Mean firing rate of all cells with at least one place field, and distribution of place field peaks (**D**). **E:** Standard deviation of single-trial tuning curves, computed across trials within a session (raw) or normalized by the mean (**F**). **G:** Entire-session tuning curve variability, estimated by a bootstrapping procedure (raw) or normalized by the mean (**H**). **I:** Raw, and z-scored (**J**) population vector correlation between tuning curves estimated across every pair of trials. **K:** Raw, and z-scored (**L**) population vector correlation between tuning curves estimated from each trial and the complementary leave-one-out tuning curves.

364 implications for the interpretation of covert activity. Specifically, different data splits did not affect decoding
 365 performance uniformly across different positions, resulting in biases that need to be taken into account when
 366 interpreting decoded “replay” data. The second contribution of this study is that for all data splits, decoding
 367 error can be substantially reduced by relatively minimal smoothing, an observation well known in other

368 fields, but not yet systematically applied to hippocampal data.

369 Both these contributions help address the question of how we should decode and interpret internally gen-
370 erated, covert activity such as occurs in hippocampal “replay” during rest and offline states. The analyses
371 presented here were performed on data from rats running on a T-maze, rather than on covert activity directly.
372 However, the crucial conceptual connection between these two is the following: because the true mapping
373 from neural activity to decoded locations that applies to internally generated activity is typically unknown
374 (see the section below for further discussion), this mapping should be optimized for generalization perfor-
375 mance. Operationally, we mimic the decoding of such covert sequences by pretending that we do not know
376 the true encoding model for specific trials on the track – by leaving out these trials in our analysis – essen-
377 tially treating them as covert sequences, but with the advantage that in this case, we can go back and evaluate
378 decoding performance.

379 To provide a specific example of how insights obtained from this procedure apply to the interpretation of
380 decoding internally generated activity: suppose we used such decoded locations to detect sequences de-
381 picting coherent trajectories along the track. We may find that these “replays” preferentially included the
382 decision point at the middle of the track, rather than the ends of the track. We may be tempted to report
383 this as a finding of interest, perhaps with an interpretation emphasizing prioritized replay as a mechanism
384 useful for reinforcement learning (Schaul et al., 2015; Gershman and Daw, 2017). However, Figure 8 should
385 make it clear that, in the data set used here, such a bias is a straightforward consequence of the increase in
386 cross-validated decoding error at both ends of the track. Crucially, if we had used same-trial decoding error
387 instead, there would not be any indication of a bias favoring the decision point.

388 Similar to the above example, it is common to use decoding analyses to support a comparison between “re-
389 play” of different experimental conditions or spatially distinct areas on the track, such as the left and right
390 arms of a T-maze (Gupta et al., 2010; Bendor and Wilson, 2012; Ólafsdóttir et al., 2015). In such compar-
391 isons, it is crucial to ensure that differences of interest in decoded trajectory counts cannot be attributed to

392 intrinsic differences in ability to decode such sequences (e.g. as a result of different distributions of firing
393 fields across locations, firing rates, etc). A common way to control for this is to compare decoding accuracy
394 during behavior across the conditions to be compared; our results show that such measures can differ sub-
395 stantially when based on tautological or cross-validated decoding. Thus, in this setting, as in the previous
396 example, *the cross-validated decoding error provides an important null hypothesis*: the distribution of replay
397 content expected from the decoder’s ability to generalize to neural activity not in the training set.

398 Note that we are not suggesting any changes to the decoding of “replay” activity itself: this can be done
399 with tuning curves obtained from the full set of behavioral data, because replay activity is not included in
400 the tuning curves. Rather, we point out that the *interpretation* of the replay decoding results should take the
401 cross-validated, not tautological, decoding accuracy during behavior on into account. Whether or not any
402 observed bias in cross-validated decoding error presents a problem depends on the alternative hypothesis
403 to be tested against the potentially non-uniform null hypothesis provided by cross-validated decoding error.
404 Following the example above: the observed bias in cross-validated decoding error to be lower around the
405 choice point of the T-maze casts doubt on the alternative hypothesis that uniform experience is transformed
406 into preferential replay of choice points. However, this same bias may not matter for determining whether
407 there exists a difference between the number of observed “left” and “right” replays.

408 We found that generalization error depends on the number of trials used to estimate the encoding model, with
409 trial numbers up to the 10 tested generally resulting in lower error. This is intuitive, as a noisy, corrupted
410 tuning curve will lead to a less effective decoder than an accurate one. Note that this implies that when
411 comparing replay content across conditions as in the examples above, the amount of data used to estimate
412 tuning curves should be equalized to eliminate bias due to this effect. As the number of trials used for cross-
413 validation becomes larger, the difference with all-to-all decoding becomes proportionally smaller. Thus, the
414 importance of reporting cross-validated error is especially key when smaller numbers of encoding trials are
415 used, a situation we expect to become more common due to factors such as more complex environments
416 that limit behavioral sampling, and limitations in imaging time due to photobleaching of reporter molecules

417 (Rubin et al., 2015; Malvache et al., 2016).

418 More trials do not always make for a better encoding model, however; this is illustrated by our observation
419 that decoding error increased when using trials that occurred further apart in time (Figure 7). As we could
420 not explain this effect based on changes in behavioral variables, this suggests a certain amount of trial-unique
421 content, as has been shown previously with different analyses (Manns et al., 2007; Mankin et al., 2012; Ziv
422 et al., 2013). If the contribution of time, or trial-unique features more generally, to internally generated
423 sequences is large (Takahashi, 2015; Schwindel et al., 2016), then averaging across many trials may limit
424 and/or bias the detection of trial-specific replay content. As it is not yet clear to what extent internally
425 generated sequences reflect trial-unique experience, it is difficult to convert this possibility into specific
426 recommendations when interpreting decoded replay data. A conservative approach would be to verify the
427 robustness of a decoding result against variations in the encoding model used (e.g. by using different subsets
428 of trials for decoding; we thank one of the referees for this suggestion).

429 Finally, beyond the comparison of different data splits discussed above, we show that regardless of split,
430 decoding error can be reduced substantially by decoding spike density functions (SDFs) rather than binned
431 spike counts. Such temporal smoothing has been shown to improve decoding of arm reaching direction from
432 motor cortex activity (Cunningham et al. 2009; see also Kass et al. 2003; Shimazaki and Shinomoto 2010;
433 Prerau and Eden 2011 for a more general treatment of statistical issues in spike rate estimation) but to our
434 knowledge this approach has not been used in studies of hippocampal place cell activity. Although numerous
435 studies have examined the effects of the size of the time window on decoding accuracy (τ ; e.g. Wilson and
436 McNaughton 1993; Zhang et al. 1998; Resnik et al. 2012; Chen et al. 2016), this is different from our spike
437 density function (SDF) estimation approach: the Gaussian kernel width used in SDF estimation can be ma-
438 nipulated independently from the window size. Thus, for a given window size, such as the 25 ms used here,
439 a variable amount of smoothing can be applied. This modification can be straightforwardly accommodated
440 in commonly used Bayesian decoding procedures (Zhang et al., 1998). Remarkably, decoding performance
441 improves even when estimating SDFs with very narrow kernels (e.g. with a standard deviation of 2 or 5 ms).

442 Using narrow kernels is particularly important for applications in decoding covert activity, which in the case
443 of hippocampal place cells is temporally compressed relative to behavioral experience (Nadasdy et al., 1999;
444 Lee and Wilson, 2002; Dragoi and Buzsáki, 2006; Buzsáki, 2015).

445 **Limitations**

446 Our suggestion that decoders intended for covert neural activity should be optimized for cross-validated
447 (generalization) performance is based on the assumption that the “true”, correct decoder for such activity
448 is unknown. Clearly, the approach taken here cannot itself determine the true mapping from covert neural
449 activity to stimulus space. Demonstrating the nature of this mapping is a challenging problem, which may
450 require grounding in experimental observations. Two promising directions may include (1) obtaining access
451 to a brain-internal decoder, such as a downstream projection target, making it possible to determine what as-
452 pects of presynaptic activity are distinguished at a next processing stage (Ji and Wilson, 2007; Lansink et al.,
453 2009; Ólafsdóttir et al., 2016; Jadhav et al., 2016); and (2) applying experimental manipulations contingent
454 on decoded content, such that any behavioral effects relative to an appropriate control would constitute ev-
455 idence that the decoder captures something relevant (clusterless decoding is a promising approach for this;
456 Kloosterman et al. 2014; Deng et al. 2015). A different approach is to construct generative models in an
457 attempt to reproduce experimentally observed activity (Johnson et al., 2008; Pfeiffer and Foster, 2015; Chen
458 et al., 2016). In the limit of a perfect match between the model output and the experimentally observed data,
459 then the optimal decoder can be determined from what is now a known ground truth (the generative model).
460 However, these approaches are not yet mature, and may remain impractical for the purpose of determining
461 the most suitable decoder in any given experiment. Thus, we provide more practical recommendations in the
462 final section.

463 A different limitation of this study is that although encoding model parameters can be optimized for decoding
464 error when the true location is known, it is unclear how the parameters obtained in this way should be applied

465 to decoding covert activity. Estimates of the temporal compression in internally generated vs. overt activity
466 range from 7-20x (Lee and Wilson, 2002; Davidson et al., 2009; Buzsáki, 2015), thus a practical starting
467 point would be to simply reduce the σ_Q found to be optimal for decoding overt behavior by a factor in that
468 range. For the data set used here this would suggest a value of $\sigma_Q = 5$ ms to be a conservative estimate.
469 Future work could provide a more principled estimate of this parameter by, for instance, using generative
470 models as outlined above.

471 Similarly, our current estimation method for tuning curves uses a relatively *ad hoc* approach of non-parametrically
472 obtaining firing rates from the data, followed by smoothing. Other work has used parametric approaches such
473 as fitting Gaussians or Zernike polynomials (Barbieri et al., 2002); such methods are completely compatible
474 with the approach we take here. Our goal in this study was not to determine which method for tuning curve
475 estimation works best; rather, the main purpose of not using raw, unsmoothed tuning curves here was to pre-
476 vent inconsistent combinations of spike counts. Looking forward, however, there are clearly opportunities
477 for improving the estimation of tuning curves, such as propagating uncertainty about estimated firing rates
478 throughout the decoding procedure, correcting for the blurring effects of theta phase precession (Lisman and
479 Redish, 2009), and taking the presence of different gamma oscillations into account (Zheng et al., 2016).

480 Finally, the results provided here are based on one specific data set. However, we emphasize that the specific
481 optimal parameters and decoding error distributions found here are not meant to be imported verbatim to
482 analysis of other data sets for which they may or may not work well; if this was the purpose of the study it
483 would indeed be important to test how consistent the inferred optima are. Rather, these results illustrate the
484 importance of choosing parameters and data splits in a principled manner, and suggests specific steps that
485 can be applied to other data sets to find parameters appropriate for that data.

486 More generally, although we used hippocampal place cell data from rodents, the ideas developed here can
487 also be applied to other systems in which covert activity can be meaningfully decoded. In rodents, these
488 include the head direction system (Peyrache et al., 2015), areas involved in the processing of decision vari-

489 ables such as orbitofrontal cortex and ventral striatum (Stott and Redish, 2014), and internal representations
490 of time (Pastalkova et al., 2008; MacDonald et al., 2013; Mello et al., 2015). Non-human primate studies
491 prominently explore the generation of motor activity related to upcoming reaching movements (Wu et al.,
492 2006; Yu et al., 2009), and ensemble recording and analysis methods are becoming increasingly common in
493 studies of decision making (Rich and Wallis, 2016). In human subjects, MEG studies have started to explore
494 the fast dynamics of thought (King and Dehaene, 2014; Bellmund et al., 2016; Kurth-Nelson et al., 2016),
495 and MVPA has revealed structure in internally generated activity in a wide range of domains (Reddy et al.,
496 2010; Brown et al., 2016). The present study suggests that the analysis of internally generated sequences
497 of hippocampal activity in rodents can interact productively with statistical approaches developed across
498 domains.

499 **Summary: three practical guidelines for the decoding and interpretation of internally gener-**
500 **ated neural activity**

501 The use of cross-validation for decoding is commonplace in human neuroimaging studies (Pereira et al.,
502 2009; Shirer et al., 2012; Varoquaux et al., 2016). Several studies performing position decoding on rodent
503 hippocampus data have used a split between training and testing data (e.g. Zhang et al. 1998; Rutishauser
504 et al. 2006; Davidson et al. 2009; Resnik et al. 2012; Agarwal et al. 2014), but this practice has not been
505 consistently applied in this field. Moreover, the motivation for reporting decoding errors based on cross-
506 validation, and its particular importance for the interpretation of internally generated activity, is typically not
507 made explicit. For the decoding of hippocampal place cell data for this purpose, we suggest the following:

- 508 • Report cross-validated, not tautological, decoding error on “running” data. This is good practice in
509 general, but particularly crucial when using decoding accuracy to reveal possible bias in the ability to
510 decode different conditions or trajectories. The cross-validated decoding error distribution should be
511 viewed as a null hypothesis for comparison with alternative hypotheses about the decoded content of

512 internally generated activity, such as replay.

513 • Because cross-validated decoding error depends (1) on the amount of data (e.g. number of trials) used
514 to estimate tuning curves, and (2) temporal distance between trials used to estimate tuning curves and
515 the time of decoding. Thus, these factors should be equalized, either by design or by subsampling,
516 when comparing replay content across conditions.

517 • Even very mild smoothing of the spike trains to be decoded, such as a 5 ms Gaussian kernel for spike
518 density functions, and a 3 cm kernel for tuning curves, can substantially improve decoding perfor-
519 mance. However, due to the compression of hippocampal replay relative to behavioral experience,
520 excessive smoothing is discouraged.

521 **Acknowledgments**

522 This work was supported by NWO, HFSP, and the Templeton Foundation (MvdM). We are grateful to Loren
523 Frank, Margaret Carr, and Caleb Kemere for sharing the original design upon which our electrode arrays
524 were based. We thank Nancy Gibson, Jean Flanagan, and Martin Ryan for assistance with animal care,
525 Harmen VanderHeide, Jacek Szubra, Andrew Dubé, and Zhenwhen Zhang for technical assistance, and
526 Min-Ching Kuo for assistance with surgery. We thank Adam Johnson, Elyot Grant and Alireza Soltani for
527 helpful comments on an earlier version of the manuscript, and the referees for insightful suggestions.

528 Author contributions: MvdM designed and supervised research. AAC performed experiments, preprocessed
529 and annotated the data. AAC, YT and MvdM wrote analysis code. MvdM performed analysis. MvdM wrote
530 the manuscript with input from AAC and YT.

531 **References**

- 532 Agarwal, G., Stevenson, I. H., Berényi, A., Mizuseki, K., Buzsáki, G., and Sommer, F. T. (2014). Spatially distributed local fields
533 in the hippocampus encode rat position. *Science*, 344(6184):626–30.
- 534 Allen, K., Rawlins, J. N. P., Bannerman, D. M., and Csicsvari, J. (2012). Hippocampal Place Cells Can Encode Multiple Trial-
535 Dependent Features through Rate Remapping. *Journal of Neuroscience*, 32(42):14752–66.
- 536 Allen, T. A., Salz, D. M., McKenzie, S., and Fortin, N. J. (2016). Nonspatial Sequence Coding in CA1 Neurons. *Journal of*
537 *Neuroscience*, 36(5):1547–1563.
- 538 Alpaydin, E. (2014). *Introduction to machine learning*. MIT press.
- 539 Barbieri, R., Frank, L. M., Quirk, M. C., Solo, V., Wilson, M. A., and Brown, E. N. (2002). Construction and analysis of non-
540 Gaussian spatial models of neural spiking activity. *Neurocomputing*, 44:309–314.
- 541 Bellmund, J. L., Deuker, L., Navarro Schröder, T., and Doeller, C. F. (2016). Grid-cell representations in mental simulation. *eLife*,
542 5:12897–12901.
- 543 Bendor, D. and Wilson, M. A. (2012). Biasing the content of hippocampal replay during sleep. *Nature neuroscience*, 15(10):1439–
544 44.
- 545 Bialek, W., Rieke, F., de Ruyter van Steveninck, R. R., and Warland, D. (1991). Reading a neural code. *Science*, 252(5014):1854–7.
- 546 Bishop, C. M. (2006). Pattern recognition. *Machine Learning*, 128.
- 547 Brown, E. N., Frank, L. M., Tang, D., Quirk, M. C., and Wilson, M. A. (1998). A statistical paradigm for neural spike train
548 decoding applied to position prediction from ensemble firing patterns of rat hippocampal place cells. *Journal of Neuroscience*,
549 18:7411–7425.
- 550 Brown, T. I., Carr, V. A., LaRocque, K. F., Favila, S. E., Gordon, A. M., Bowles, B., Bailenson, J. N., and Wagner, A. D. (2016).
551 Prospective representation of navigational goals in the human hippocampus. *Science*, 352(6291):1323–6.
- 552 Buzsáki, G. (2015). Hippocampal sharp wave-ripple: A cognitive biomarker for episodic memory and planning. *Hippocampus*,
553 25(10):1073–188.
- 554 Carr, M. F., Jadhav, S. P., and Frank, L. M. (2011). Hippocampal replay in the awake state: a potential substrate for memory
555 consolidation and retrieval. *Nature Neuroscience*, 14(2):147–53.
- 556 Chadwick, A., van Rossum, M. C., and Nolan, M. F. (2015). Independent theta phase coding accounts for CA1 population sequences
557 and enables flexible remapping. *eLife*, 4.
- 558 Chen, Z., Grosmark, A. D., Penagos, H., and Wilson, M. A. (2016). Uncovering representations of sleep-associated hippocampal
559 ensemble spike activity. *Scientific reports*, 6:32193.
- 560 Cunningham, J. P., Gilja, V., Ryu, S. I., and Shenoy, K. V. (2009). Methods for estimating neural firing rates, and their application
561 to brainmachine interfaces. *Neural Networks*, 22(9):1235–1246.

- 562 Davidson, T. J., Kloosterman, F., and Wilson, M. A. (2009). Hippocampal replay of extended experience. *Neuron*, 63(4):497–507.
- 563 Deng, X., Liu, D. F., Kay, K., Frank, L. M., and Eden, U. T. (2015). Clusterless Decoding of Position from Multiunit Activity Using
564 a Marked Point Process Filter. *Neural Computation*, 27(7):1438–1460.
- 565 Dragoi, G. and Buzsáki, G. (2006). Temporal encoding of place sequences by hippocampal cell assemblies. *Neuron*, 50(1):145–57.
- 566 Dragoi, G. and Tonegawa, S. (2013). Distinct preplay of multiple novel spatial experiences in the rat. *Proceedings of the National
567 Academy of Sciences*, 110(22):9100–9105.
- 568 Feng, T., Silva, D., and Foster, D. J. (2015). Dissociation between the experience-dependent development of hippocampal theta
569 sequences and single-trial phase precession. *Journal of Neuroscience*, 35(12):4890–902.
- 570 Foster, D. J. and Wilson, M. A. (2007). Hippocampal theta sequences. *Hippocampus*, 17(11):1093–9.
- 571 Georgopoulos, A. P., Lurito, J. T., Petrides, M., Schwartz, A. B., and Massey, J. T. (1989). Mental rotation of the neuronal population
572 vector. *Science*, 243(4888):234–6.
- 573 Georgopoulos, A. P., Schwartz, A. B., and Kettner, R. E. (1986). Neuronal population coding of movement direction. *Science*,
574 233:1416–1419.
- 575 Gershman, S. J. and Daw, N. D. (2017). Reinforcement Learning and Episodic Memory in Humans and Animals: An Integrative
576 Framework. *Annual Review of Psychology*, 68(1):101–128.
- 577 Girardeau, G., Benchenane, K., Wiener, S. I., Buzsáki, G., and Zugaro, M. B. (2009). Selective suppression of hippocampal ripples
578 impairs spatial memory. *Nature Neuroscience*, 12(10):1222–3.
- 579 Grosmark, A. D. and Buzsáki, G. (2016). Diversity in neural firing dynamics supports both rigid and learned hippocampal sequences.
580 *Science*, 351(6280):1440–1443.
- 581 Gupta, A. S., van der Meer, M. A. A., Touretzky, D. S., and Redish, A. D. (2010). Hippocampal replay is not a simple function of
582 experience. *Neuron*, 65(5):695–705.
- 583 Gupta, A. S., van der Meer, M. A. A., Touretzky, D. S., and Redish, A. D. (2012). Segmentation of spatial experience by hippocampal
584 θ sequences. *Nature Neuroscience*, 15(7):1032–9.
- 585 Hawkins, D. M. (2004). The Problem of Overfitting.
- 586 Huxter, J., Burgess, N., and O’Keefe, J. (2003). Independent rate and temporal coding in hippocampal pyramidal cells. *Nature*,
587 425(6960):828.
- 588 Jadhav, S., Rothschild, G., Roumis, D., and Frank, L. (2016). Coordinated Excitation and Inhibition of Prefrontal Ensembles during
589 Awake Hippocampal Sharp-Wave Ripple Events. *Neuron*, 90(1):113–127.
- 590 Jadhav, S. P., Kemere, C., German, P. W., and Frank, L. M. (2012). Awake hippocampal sharp-wave ripples support spatial memory.
591 *Science*, 336(6087):1454–8.
- 592 Ji, D. and Wilson, M. A. (2007). Coordinated memory replay in the visual cortex and hippocampus during sleep. *Nature Neuro-
593 science*, 10(1):100–107.

- 594 Johnson, A., Fenton, A. A., Kentros, C., and Redish, A. D. (2009). Looking for cognition in the structure within the noise. *Trends*
595 *in cognitive sciences*, 13(2):55–64.
- 596 Johnson, A., Jackson, J., and Redish, A. D. (2008). Measuring distributed properties of neural representations beyond the decoding
597 of local variables — implications for cognition. In Hölscher, C. and Munk, M. H. J., editors, *Mechanisms of information*
598 *processing in the Brain: Encoding of information in neural populations and networks*, pages 95–119. Cambridge University
599 Press.
- 600 Johnson, A. and Redish, A. D. (2007). Neural ensembles in CA3 transiently encode paths forward of the animal at a decision point.
601 *Journal of Neuroscience*, 27(45):12176–12189.
- 602 Káli, S. and Dayan, P. (2004). Off-line replay maintains declarative memories in a model of hippocampal-neocortical interactions.
603 *Nature neuroscience*, 7(3):286–94.
- 604 Karlsson, M. P. and Frank, L. M. (2009). Awake replay of remote experiences in the hippocampus. *Nature Neuroscience*, 12(7):913–
605 8.
- 606 Kass, R. E., Eden, U. T., and Brown, E. N. (2014). *Analysis of neural data*. Springer.
- 607 Kass, R. E., Ventura, V., and Cai, C. (2003). Statistical smoothing of neuronal data. *Comput. Neural Syst*, 14:5–15.
- 608 King, J.-R. and Dehaene, S. (2014). Characterizing the dynamics of mental representations: the temporal generalization method.
609 *Trends in Cognitive Sciences*, 18(4):203–210.
- 610 Kloosterman, F. (2012). Analysis of hippocampal memory replay using neural population decoding. *Neuronal Network Analysis:*
611 *Concepts and Experimental Approaches*, pages 259–282.
- 612 Kloosterman, F., Layton, S. P., Chen, Z., and Wilson, M. A. (2014). Bayesian decoding using unsorted spikes in the rat hippocampus.
613 *Journal of neurophysiology*, 111(1):217–27.
- 614 Kurth-Nelson, Z., Economides, M., Dolan, R., and Dayan, P. (2016). Fast Sequences of Non-spatial State Representations in
615 Humans. *Neuron*, 91(1):194–204.
- 616 Lansink, C. S., Goltstein, P. M., Lankelma, J. V., McNaughton, B. L., and Pennartz, C. M. A. (2009). Hippocampus leads ventral
617 striatum in replay of place-reward information. *PLoS Biol*, 7(8):e1000173.
- 618 Lee, A. K. and Wilson, M. A. (2002). Memory of sequential experience in the hippocampus during slow wave sleep. *Neuron*,
619 36(6):1183–1194.
- 620 Lin, L., Osan, R., Shoham, S., Jin, W., Zuo, W., and Tsien, J. Z. (2005). Identification of network-level coding units for real-time
621 representation of episodic experiences in the hippocampus. *Proceedings of the National Academy of Sciences*, 102(17):6125–
622 6130.
- 623 Lisman, J. and Redish, A. (2009). Prediction, sequences and the hippocampus. *Philosophical transactions of the Royal Society of*
624 *London. Series B, Biological sciences*, 364(1521):1193–201.
- 625 MacDonald, C. J., Carrow, S., Place, R., and Eichenbaum, H. (2013). Distinct Hippocampal Time Cell Sequences Represent Odor

- 626 Memories in Immobilized Rats. *Journal of Neuroscience*, 33(36):14607–14616.
- 627 Malhotra, S., Cross, R. W., and van der Meer, M. A. A. (2012). Theta phase precession beyond the hippocampus. *Reviews in the*
628 *Neurosciences*, 23(1):39–65.
- 629 Malhotra, S., Cross, R. W., Zhang, A., and Van Der Meer, M. A. A. (2015). Ventral striatal gamma oscillations are highly variable
630 from trial to trial, and are dominated by behavioural state, and only weakly influenced by outcome value. *European Journal of*
631 *Neuroscience*, 42(10):2818–2832.
- 632 Malvache, A., Reichinnek, S., Villette, V., Haimerl, C., and Cossart, R. (2016). Awake hippocampal reactivations project onto
633 orthogonal neuronal assemblies. *Science*, 353(6305).
- 634 Mankin, E. A., Sparks, F. T., Slayyeh, B., Sutherland, R. J., Leutgeb, S., and Leutgeb, J. K. (2012). Neuronal code for extended
635 time in the hippocampus. *Proceedings of the National Academy of Sciences of the United States of America*, 109(47):19462–7.
- 636 Manns, J. R., Howard, M. W., and Eichenbaum, H. (2007). Gradual Changes in Hippocampal Activity Support Remembering the
637 Order of Events. *Neuron*, 56(3):530–540.
- 638 McClelland, J. L., McNaughton, B. L., and O'Reilly, R. C. (1995). Why there are complementary learning systems in the hippocam-
639 pus and neocortex: insights from the successes and failures of connectionist models of learning and memory. *Psychological*
640 *review*, 102(3):419–57.
- 641 McKenzie, S., Frank, A., Kinsky, N., Porter, B., Rivière, P., and Eichenbaum, H. (2014). Hippocampal Representation of Related
642 and Opposing Memories Develop within Distinct, Hierarchically Organized Neural Schemas. *Neuron*, 83(1):202–215.
- 643 Mello, G., Soares, S., and Paton, J. (2015). A Scalable Population Code for Time in the Striatum. *Current Biology*, 25(9):1113–1122.
- 644 Nadasdy, Z., Hirase, H., Czurko, A., Csicsvari, J., and Buzsáki, G. (1999). Replay and time compression of recurring spike
645 sequences in the hippocampus. *J Neurosci*, 19(21):9497–9507.
- 646 Nirenberg, S. and Latham, P. E. (2003). Decoding neuronal spike trains: How important are correlations? *Proceedings of the*
647 *National Academy of Sciences*, 100(12):7348–7353.
- 648 Ólafsdóttir, H. F., Barry, C., Saleem, A. B., Hassabis, D., and Spiers, H. J. (2015). Hippocampal place cells construct reward related
649 sequences through unexplored space. *eLife*, 4:e06063.
- 650 Ólafsdóttir, H. F., Carpenter, F., and Barry, C. (2016). Coordinated grid and place cell replay during rest. *Nature Neuroscience*,
651 19(6):792–794.
- 652 O'Neill, J., Senior, T., and Csicsvari, J. (2006). Place-selective firing of CA1 pyramidal cells during sharp wave/ripple network
653 patterns in exploratory behavior. *Neuron*, 49(1):143–155.
- 654 Panzeri, S., Macke, J. H., Gross, J., and Kayser, C. (2015). Neural population coding: combining insights from microscopic and
655 mass signals. *Trends in cognitive sciences*, 19(3):162–72.
- 656 Pastalkova, E., Itskov, V., Amarasingham, A., and Buzsáki, G. (2008). Internally generated cell assembly sequences in the rat
657 hippocampus. *Science*, 321(5894):1322–7.

- 658 Pereira, F., Mitchell, T., and Botvinick, M. (2009). Machine learning classifiers and fMRI: a tutorial overview.
- 659 Peyrache, A., Lacroix, M. M., Petersen, P. C., and Buzsáki, G. (2015). Internally organized mechanisms of the head direction sense.
660 *Nature Neuroscience*, 18(4):569–75.
- 661 Pfeiffer, B. E. and Foster, D. J. (2013). Hippocampal place-cell sequences depict future paths to remembered goals. *Nature*,
662 497(7447):74–9.
- 663 Pfeiffer, B. E. and Foster, D. J. (2015). Autoassociative dynamics in the generation of sequences of hippocampal place cells. *Science*,
664 349(6244):180–183.
- 665 Pillow, J. W., Ahmadian, Y., and Paninski, L. (2011). Model-based decoding, information estimation, and change-point detection
666 techniques for multineuron spike trains. *Neural computation*, 23(1):1–45.
- 667 Pillow, J. W., Shlens, J., Paninski, L., Sher, A., Litke, A. M., Chichilnisky, E. J., and Simoncelli, E. P. (2008). Spatio-temporal
668 correlations and visual signalling in a complete neuronal population. *Nature*, 454(7207):995–999.
- 669 Prerau, M. J. and Eden, U. T. (2011). A General Likelihood Framework for Characterizing the Time Course of Neural Activity.
670 *Neural Computation*, 23(10):2537–2566.
- 671 Reddy, L., Tsuchiya, N., and Serre, T. (2010). Reading the mind’s eye: Decoding category information during mental imagery.
672 *NeuroImage*, 50(2):818–825.
- 673 Resnik, E., McFarland, J. M., Sprengel, R., Sakmann, B., and Mehta, M. R. (2012). The Effects of GluA1 Deletion on the
674 Hippocampal Population Code for Position. *Journal of Neuroscience*, 32(26).
- 675 Rich, E. L. and Wallis, J. D. (2016). Decoding subjective decisions from orbitofrontal cortex. *Nature Neuroscience*, 19(7):973–980.
- 676 Rubin, A., Geva, N., Sheintuch, L., and Ziv, Y. (2015). Hippocampal ensemble dynamics timestamp events in long-term memory.
677 *eLife*, 4:723–727.
- 678 Rutishauser, U., Mamelak, A. N., and Schuman, E. M. (2006). Single-Trial Learning of Novel Stimuli by Individual Neurons of the
679 Human Hippocampus-Amygdala Complex.
- 680 Schaul, T., Quan, J., Antonoglou, I., and Silver, D. (2015). Prioritized Experience Replay. *ArXiv 1511.05952*.
- 681 Schneidman, E. (2016). Towards the design principles of neural population codes. *Current opinion in neurobiology*, 37:133–140.
- 682 Schwindel, C. D., Navratilova, Z., Ali, K., Tatsuno, M., and McNaughton, B. L. (2016). Reactivation of Rate Remapping in CA3.
683 *Journal of Neuroscience*, 36(36).
- 684 Shimazaki, H. and Shinomoto, S. (2010). Kernel bandwidth optimization in spike rate estimation. *Journal of Computational*
685 *Neuroscience*, 29(1-2):171–182.
- 686 Shirer, W. R., Ryali, S., Rykhlevskaia, E., Menon, V., and Greicius, M. D. (2012). Decoding subject-driven cognitive states with
687 whole-brain connectivity patterns. *Cerebral Cortex*, 22(1):158–165.
- 688 Silva, D., Feng, T., and Foster, D. J. (2015). Trajectory events across hippocampal place cells require previous experience. *Nature*
689 *Neuroscience*, 18(12):1772–1779.

- 690 Skaggs, W. E. and McNaughton, B. L. (1996). Replay of neuronal firing sequences in rat hippocampus during sleep following
691 spatial experience. *Science*, 271(5257):1870–3.
- 692 Stott, J. J. and Redish, A. D. (2014). A functional difference in information processing between orbitofrontal cortex and ventral
693 striatum during decision-making behaviour. *Philosophical transactions of the Royal Society of London. Series B, Biological*
694 *sciences*, 369(1655):199–204.
- 695 Takahashi, S. (2015). Episodic-like memory trace in awake replay of hippocampal place cell activity sequences. *Elife*, 4:e08105.
- 696 Tatsuno, M., Lipa, P., and McNaughton, B. L. (2006). Methodological Considerations on the Use of Template Matching to Study
697 Long-Lasting Memory Trace Replay. *Journal of Neuroscience*, 26(42):10727–10742.
- 698 van der Meer, M. A. A., Johnson, A., Schmitzer-Torbert, N. C., and Redish, A. D. (2010). Triple Dissociation of Information
699 Processing in Dorsal Striatum, Ventral Striatum, and Hippocampus on a Learned Spatial Decision Task. *Neuron*, 67(1):25–32.
- 700 Varoquaux, G., Raamana, P., Engemann, D., Hoyos-Idrobo, A., Schwartz, Y., and Thirion, B. (2016). Assessing and tuning brain
701 decoders: cross-validation, caveats, and guidelines. *arXiv:1606.05201 [stat.ML]*.
- 702 Wilson, M. A. and McNaughton, B. L. (1993). Dynamics of the hippocampal ensemble code for space. *Science*, 261:1055–1058.
- 703 Wu, W., Gao, Y., Bienenstock, E., Donoghue, J. P., and Black, M. J. (2006). Bayesian Population Decoding of Motor Cortical
704 Activity Using a Kalman Filter. *Neural Computation*, 18(1):80–118.
- 705 Yu, B. M., Cunningham, J. P., Santhanam, G., Ryu, S. I., Shenoy, K. V., and Sahani, M. (2009). Gaussian-process factor analysis
706 for low-dimensional single-trial analysis of neural population activity. *Journal of neurophysiology*, 102(1):614–35.
- 707 Zhang, K., Ginzburg, I., McNaughton, B. L., and Sejnowski, T. J. (1998). Interpreting Neuronal Population Activity by Reconstruc-
708 tion: Unified Framework With Application to Hippocampal Place Cells. *Journal of Neurophysiology*, 79:1017–1044.
- 709 Zheng, C., Bieri, K., Hsiao, Y.-T., and Colgin, L. (2016). Spatial Sequence Coding Differs during Slow and Fast Gamma Rhythms
710 in the Hippocampus. *Neuron*, 89(2):398–408.
- 711 Ziv, Y., Burns, L. D., Cocker, E. D., Hamel, E. O., Ghosh, K. K., Kitch, L. J., Gamal, A. E., and Schnitzer, M. J. (2013). Long-term
712 dynamics of CA1 hippocampal place codes. *Nature Neuroscience*, 16(3):264–266.